Noise-related resolution limit of dispersion measurements with white-light interferometers

Anastassia Gosteva, Markus Haiml, Ruediger Paschotta, and Ursula Keller

Department of Physics, ETH Zurich, Institute of Quantum Electronics Wolfgang-Pauli-Strasse 16, CH-8093 Zurich, Switzerland

Received November 18, 2004; revised manuscript received March 31, 2005; accepted April 12, 2005

This paper presents results of our detailed theoretical and experimental analysis of the relationship between the spectral resolution and the noise in the group-delay dispersion (GDD) data measured by scanning white-light interferometry. We demonstrate that the practically achievable spectral resolution is limited, because the standard deviation of GDD is proportional to the third power of inverse spectral resolution, and for a specified accuracy the required number of averages scales with the sixth power of inverse spectral resolution. The influence of experimental parameters such as spectral brightness, bandwidth of the light source, and detection noise is examined in detail. © 2005 Optical Society of America

OCIS codes: 120.3180, 260.2030, 120.5050, 320.0320.

1. INTRODUCTION

Precise knowledge of the group delay dispersion (GDD) of optical components plays a central role in the generation, propagation, and characterization of ultrashort laser pulses.[1] The GDD is the second derivative of the optical phase delay with respect to the angular frequency ω. Presence of GDD leads to temporal pulse broadening and chirping; therefore the accuracy of GDD determination is particularly critical for intracavity elements of passively mode-locked lasers with pulse durations in the few-cycle regime,[2–4] for supercontinuum generation in fibers,[5,6] and ultrabroadband compression.[7–13] The exact knowledge of GDD is also important for optical-pulse-characterization techniques[14–16] involving optical elements such as beam splitters, lenses, and mirrors. Narrow-bandwidth resonances of Gires–Tournois interferometers, as frequently used in soliton mode-locked lasers operating in the picosecond regime, are also the subject of dispersion characterization. At the operation wavelength of vertical-external-cavity, surface-emitting semiconductor lasers[17,18] and semiconductor saturable absorber mirrors,[19] narrowband phase oscillations might also occur, depending on the device design. Even for picosecond lasers, the dispersion effects can sometimes be important and may have to be measured. In general, dispersion characterization is a valuable tool for post-growth design control of dielectric or epitaxially grown multilayer devices.

The standard way in which GDD is measured is via white-light interferometry. Here, the output of a broadband light source is fed into the interferometer, typically of Michelson type. The device under test (DUT) is placed in the sample arm, whereas the reference arm contains optics with known dispersion. The resulting interference pattern is monitored either with a photodiode (time-domain sampling, spectrally integrated detection)[20,21] or using spectral interferometry.[22–26] The obvious advantage of the spectrally integrated method is that the phase is evaluated simultaneously for all frequency components, so even a light source with low-power spectral density can be used. In comparison with the spectrally resolved detection, the spectrally integrated method does not require monochromators, spectrometers, or detector arrays; therefore there is no need in otherwise necessary calibration of these devices.[27] Low equipment cost and the possibility of real-time alignment of tilt and zero delay monitoring make the temporal detection methods particularly attractive. The present paper is focused mostly on scanning Michelson white-light interferometers with spectrally integrated temporal detection and Fourier transform analysis. The results of this research can be adopted for spectrally resolved interferometry (some comments on spectrally resolved interferometry are given in Section 6); however, a detailed comparison between spectrally resolved and spectrally integrated detection methods goes beyond the scope of this paper.

Spectral resolution, the accuracy of GDD determination, and the measurement time are the key parameters of every dispersion measurement. As with any Fourier spectrometer, the spectral resolution is determined by the inverse of the total scanning range (or time delay) over which data are recorded. The data are affected by noise from the light source and from detection electronics, causing a random inaccuracy in the measured GDD; this inaccuracy can be reduced by properly averaging the results of repeated measurements. By increasing the scanning range, one can achieve a better wavelength resolution, but at the same time this strongly increases the sensitivity to noise, as we will show below. Therefore, for a certain required accuracy of the GDD measurement, the required measurement time critically depends on the spectral resolution.

Depending on the specific application, the requirements of dispersion measurements may vary. For example, GDD measurements of optics employed in few-cycle pulse generation or characterization must be

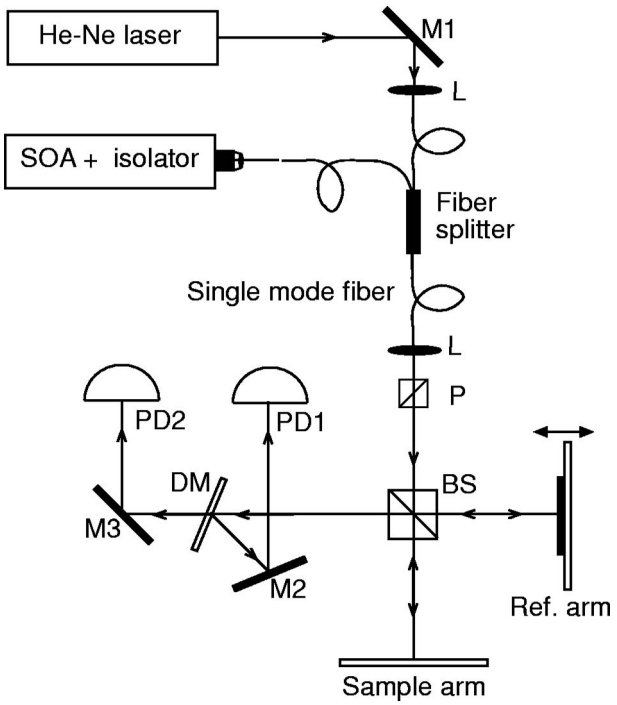

Fig. 1. Scanning Michelson interferometer using a fiber-coupled white-light source with the peak spectral brightness at 1550 nm. M1, M2, and M3 are silver mirrors; SOA = semiconductor optical amplifier (50 nm FWHM, 3 μW/nm); L = lens; P = polarizer; BS = nonpolarizing beam splitter; PD1 = silicon photodiode; PD2 = InGaAs photodiode; DM = dichroic mirror.

performed with an accuracy of a few fs^2 or better over several hundred nanometers of optical bandwidth, with a wavelength resolution of typically a few nanometers. In this paper we describe an experimental setup for reliable and accurate determination of GDD values in this regime and discuss the relation between spectral resolution and precision of GDD measurement. We present analytical calculations as well as experimental data, which confirm our analytical results quantitatively. Section 6 also addresses the impact of the spectral power density and the bandwidth of the light source.

2. EXPERIMENTAL SETUP

To simplify the alignment procedure, we constructed a fiber-coupled, collinear setup with two light sources, as shown in Fig. 1. For measurements around 1550 nm we use the amplified spontaneous emission of a fiber-coupled semiconductor optical amplifier (SOA) with a 50 nm FWHM broad Gaussian spectrum and a maximum spectral power density of 3 μW/nm. Sinusoidal movements of the reference mirror with a frequency of approximately 9 Hz are achieved with a home-built shaking system. The travel distances of the reference arm were approximately 130, 210, and 300 μm, depending on the spectral resolution (9.1, 5.8, and 4.0 nm). The interferometric trace is detected with an InGaAs photodiode (Thorlabs PDA400, 700 kHz, 75 $\times$ 10^3 V/A) and recorded with a fast oscilloscope (LeCroy WavePro 7000, 9.5 bit vertical resolution, 100 MSamples/s). An accurate determination of the time-dependent delay position is obtained from an interferogram of a 632.8 nm He–Ne laser recorded with a separate Si photodiode (Thorlabs PDA55). From the He–Ne trace at the oscilloscope, we extract the actual delay of each sample point and interpolate the signal interferogram using 16 384 points evenly spaced in position delay. Since both interferograms are recorded simultaneously, the influence of mechanical vibrations of optical components up to several 10 kHz can be eliminated. We use a tapered dichroic fiber splitter (Fiber Resources) to combine both beams at the input port of the free-space interferometer. The high update rate of ~3 Hz and the visible He–Ne beam simplify the tilt and zero-delay adjustment of the week infrared white-light beam. Both beams are separated by a dichroic mirror after the interferometer. Owing to the different spectral sensitivities of the Si and InGaAs photodiodes, no crosstalk in the recording of the two interferograms can occur.

3. ALGORITHM FOR RETRIEVING THE DISPERSION

Let us consider a white-light source with the spectral power density $S(\omega)$ and (unknown and random) frequency-dependent phase $\varphi_{\mathrm{wl}}(\omega)$ illuminating a Michelson interferometer, whose arms are of nearly equal length z_1 and z_2. The arm length difference is $\Delta z = (z_2 - z_1)$. For simplicity we assumed that the beam splitter has a frequency-independent reflectivity and introduces no phase changes. The DUT is inserted into the sample arm, for instance as a folding mirror for GDD measurements of optics used under a certain angle, or as a retroreflector for normal incidence measurements. The amplitude of the electric field emitted by the source at the entrance of the interferometer ($z = 0$) can be written as

$$E(t) \propto \int_{-\infty}^{+\infty} \sqrt{S(\omega)} \exp[i\omega t + i\varphi_{\mathrm{wl}}(\omega)] \mathrm{d}\omega. \tag{1}$$

Assuming a linear propagation regime, the time-varying contributions to the detected electric field from each arm of the interferometer are given by

$$E_1(z_1,t) \propto \int_{-\infty}^{+\infty} \sqrt{S(\omega)} r_{\mathrm{ref}}(\omega) \exp\left[i\omega\left(t - \frac{z_1}{c} \right) + i\varphi_{\mathrm{wl}}(\omega) \right] \mathrm{d}\omega, \tag{2}$$

$$E_2(z_2,t) \propto \int_{-\infty}^{+\infty} \sqrt{S(\omega)} r_{\mathrm{sa}}(\omega) \exp\left[\mathrm{i}\omega\left(t - \frac{z_2}{c} \right) + i\varphi_{\mathrm{wl}}(\omega) \right] \mathrm{d}\omega, \tag{3}$$

where $r_{\mathrm{ref}}(\omega)$ and $r_{\mathrm{sa}}(\omega)$ are the frequency-dependent complex amplitude reflectivity of the reference arm and the sample arm, respectively.

The intensity of the output field detected by a photodiode is proportional to the squared modulus of the sum of the reference and sample fields at the output:

$$I(\Delta z) \propto \langle |E_1(z_1,t)|^2 + |E_2(z_2,t)|^2 + E_1^*(z_1,t)E_2(z_2,t) + E_1(z_1,t)E_2^*(z_2,t) \rangle, \tag{4}$$

where angle brackets correspond to temporal averaging.

The terms independent of the position delay Δz [i.e., the first and second terms in Eq. (4)] do not contain any phase information about the sample, but they do contribute to the total noise level. The interference effect between the two fields is described by the last two terms in Eq. (4):

$$I_{\mathrm{int}}(\Delta z) \propto \langle \mathrm{Re}\{E_1^*(z_1)E_2(z_2)\}\rangle. \tag{5}$$

Taking into account the frequency δ correlation

$$\langle \exp(i\omega_1 t - i\omega_2 t)\rangle = \delta(\omega_1 - \omega_2), \tag{6}$$

the interference term of Eq. (5) can be expressed as

$$\begin{aligned} I_{\mathrm{int}}(\Delta z) &\propto \mathrm{Re}\left\{\int_{-\infty}^{+\infty} S(\omega) r_{\mathrm{ref}}^*(\omega) r_{\mathrm{sa}}(\omega) \exp\left(i\frac{\omega}{c}\Delta z\right) \mathrm{d}\omega\right\} \\ &= \mathrm{Re}\left\{\int_{-\infty}^{+\infty} S(\omega)|r_{\mathrm{ref}}||r_{\mathrm{sa}}| \exp[i\varphi_{\mathrm{sa}}(\omega) \right. \\ &\quad \left. - i\varphi_{\mathrm{ref}}(\omega)] \exp\left(i\frac{\omega}{c}\Delta z\right) \mathrm{d}\omega\right\}, \end{aligned} \tag{7}$$

where $\varphi_{\mathrm{sa}}(\omega)$ and $\varphi_{\mathrm{ref}}(\omega)$ are the phase changes in the sample and the reference arm, respectively. As it can be seen from Eq. (7), the initial phase of the white light φ_{wl} does not influence the interferogram; therefore any phase changes before and after the interferometer arms do not influence the measured dispersion. The interferometric trace is sensitive only to the relative phase change between the arms and is determined by the complex reflectivity $r_{\mathrm{ref}}(\omega)$ and $r_{\mathrm{sa}}(\omega)$.

Fourier transforming the time-domain signal into the frequency domain

$$I_{\mathrm{int}}\left(\frac{\omega}{c}\right) = \mathrm{FT}\{I_{\mathrm{int}}(\Delta z)\}, \tag{8}$$

where FT stands for Fourier transform, we extract the phase $\varphi(\omega)$ from the complex spectrum $I_{\mathrm{int}}(\omega/c)$ which consists of

$$\varphi(\omega) = \varphi_{\mathrm{sa}}(\omega) - \varphi_{\mathrm{ref}}(\omega) = \varphi_{\mathrm{DUT}}(\omega) + \varphi_{\mathrm{sa,balance}}(\omega) - \varphi_{\mathrm{ref}}(\omega), \tag{9}$$

where $\varphi_{\mathrm{DUT}}(\omega)$ is the phase shift due to the DUT and $\varphi_{\mathrm{sa,balance}}(\omega)$ corresponds to additional dispersion of the sample arm, e.g., from additional folding mirrors. To obtain $\varphi_{\mathrm{DUT}}(\omega)$, a calibration measurement without the DUT inserted into the sample arm is required. Note that $\varphi(\omega)$ has a meaningful value only where the spectral power density is sufficiently large.

We define a frequency dependent $D_2[\omega]$ as the second-order dispersion (GDD), which can be evaluated by numerical differentiation of the Fourier phase with respect to ω (here and later the square brackets refer to the values of discrete FT sampling frequencies with the spacing $\delta\omega$):

$$D_2[\omega] = \frac{\varphi[\omega + \delta\omega] - 2\varphi[\omega] + \varphi[\omega - \delta\omega]}{\delta\omega^2}. \tag{10}$$

Each D_2 value is affected by noise of the retrieved φ values. We emphasize that noise reduction should not be achieved by data smoothing of the spectral phase, since this would reduce the wavelength resolution of the measurement. Also, one should not average subsequently recorded interferograms, because this procedure would be sensitive to interferometer drifts. Instead, one should use averaging of the unwrapped phase $\varphi[\omega]$ or the D_2 values obtained from multiple data traces, subsequently taken under identical conditions, even though this requires multiple Fourier transforms. Note that the averaging of original (wrapped) phases obtained from the FT leads to the strong artificial oscillations of D_2 at the wrapping point. Averaging the unwrapped phase requires the phase noise $\sigma_\varphi[\omega] \ll \pi$; this condition identifies the spectral region with the meaningful values of measured GDD.

Application of fast Fourier transform algorithms requires equidistantly spaced data. However, even with a rather precise translation stage, this cannot be accomplished directly. We therefore simultaneously record in equidistant time intervals both the white-light interference signal and the signal obtained with the abovementioned He–Ne laser. In this way, the data points are sampled at nonequidistant positions. The exact positions are obtained with a common phase-retrieval algorithm[28] from the He–Ne trace. Subsequently, the data points are interpolated for equidistant positions. This procedure has two important advantages over triggered sampling only at zero crossings of the ac-coupled He–Ne beat; mechanical noise can be eliminated up to several tens of kilohertz (even if significant amplitude noise on the He–Ne beat is present), and we can apply oversampling in the time domain to avoid aliasing of spectral components with shorter wavelengths than the reference laser (633 nm). The latter is particularly important for performing the dispersion measurements in the visible and near-IR regimes (for example, near 800 nm) with the single-mode reference laser in IR (for example, 1.5 μm distributed-feedback laser).

4. IMPACT OF NOISE

To preserve the highest possible spectral resolution of GDD, we calculate the second derivative of the phase $\varphi(\omega)$ according to Eq. (10), where the spectral resolution $\delta\omega$ (spacing in frequency interval) is given by the inverse scanning length.

If the phase values are subject to *uncorrelated* Gaussian noise with variance σ_φ^2, the GDD variance σ_{D2}^2 can be found as

$$\begin{aligned} \sigma_{\mathrm{D2}}^2(\omega) &= \left[\frac{\mathrm{d}D_2[\omega]}{\mathrm{d}(\varphi[\omega + \delta\omega])}\sigma_\varphi[\omega + \delta\omega]\right]^2 + \left[\frac{\mathrm{d}D_2[\omega]}{\mathrm{d}(\varphi[\omega])}\sigma_\varphi[\omega]\right]^2 \\ &\quad + \left[\frac{\mathrm{d}D_2[\omega]}{\mathrm{d}(\varphi[\omega - \delta\omega])}\sigma_\varphi[\omega - \delta\omega]\right]^2 = \frac{6\sigma_\varphi^2(\omega)}{\delta\omega^4}. \end{aligned} \tag{11}$$

The spectrum of the Fourier-transformed interferogram can be described with a complex mean amplitude $\bar{s}(\omega)$ and a complex noise variance $\sigma_{\bar{s}}^2(\omega)$. For weak noise distributed evenly over both quadrature components, the amplitude noise variance $\sigma_a^2(\omega)$ is given by

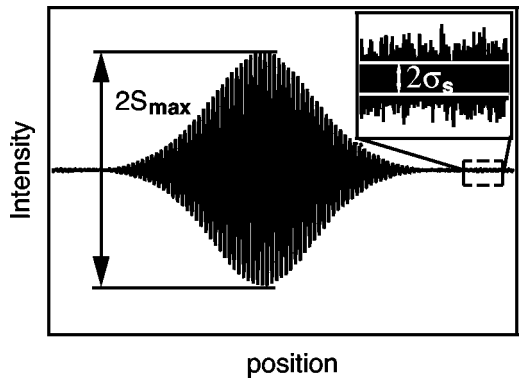

Fig. 2. Measured interferogram for a Gaussian source spectrum and low dispersion. The noise floor can be determined from the outer parts of the trace (see inset).

$$\sigma_a^2(\omega)\mathrm{d}\omega = \frac{1}{2}\sigma_{\tilde{s}}^2(\omega)\mathrm{d}\omega \tag{12}$$

and the phase noise variance $\sigma_\varphi^2(\omega)$ by

$$\sigma_\varphi^2(\omega)\mathrm{d}\omega = \frac{1}{2}\arctan\left[\frac{\sigma_{\tilde{s}}^2(\omega)\mathrm{d}\omega}{|\tilde{s}^2(\omega)|}\right] \cong \frac{\sigma_{\tilde{s}}^2(\omega)\mathrm{d}\omega}{2|\tilde{s}^2(\omega)|}. \tag{13}$$

Now we have to clarify how the power-noise variance σ_s^2 in the time domain relates to the complex noise variance $\sigma_{\tilde{s}}^2$ in the spectral domain. If the sampling rate is well below the inverse noise bandwidth, the Parseval theorem can be applied. With the number of sampling points p, the total measurement bandwidth is $p\,\delta\omega$, and therefore the power noise variance in the spectral domain is

$$\sigma_{\tilde{s}}^2(\omega) = \frac{(2\pi)^2\sigma_s^2(t)}{p(\delta\omega)^2}. \tag{14}$$

We define the signal-to-noise ratio (SNR) in the time domain as

$$\mathrm{SNR} = S_{\max}^2/\sigma_s^2, \tag{15}$$

where

$$S_{\max} \cong \frac{1}{2\pi}\int |\tilde{s}(\omega)|\mathrm{d}\omega = \frac{1}{2\pi}\int I(\omega)\mathrm{d}\omega \tag{16}$$

estimates the maximum amplitude of the cross-correlation envelope (see Fig. 2) and $I(\omega)$ is the spectral power density. These estimates are rather accurate when the amount of dispersion to be measured is relatively small, so the shape of the cross-correlation envelope remains almost unchanged as compared to an empty zero-dispersion measurement.

By combining these results, we finally obtain for the standard deviation σ_{D2} of the measured GDD data

$$\sigma_{D2}(\omega) = \left\{3\frac{\left[\int I(\omega)\mathrm{d}\omega\right]^2}{I^2(\omega)}\frac{1}{\mathrm{SNR}\,pM(\delta\omega)^6}\right\}^{1/2}, \tag{17}$$

where we have introduced the factor M in the dominator, which takes into account the averaging of M data traces.

For some spectral shapes, Eq. (17) can be simplified further. For example, using a normalized source spectrum $I_n(\omega)$ in case of a Gaussian spectral shape with a FWHM $\Delta\omega$, the standard deviation is given by

$$\sigma_{D2}(\omega) = \left[\frac{3\pi}{4\ln(2)}\frac{1}{I_n^2(\omega)}\frac{\Delta\omega^2}{\mathrm{SNR}\,pM(\delta\omega)^6}\right]^{1/2}, \tag{18}$$

and for a flat-top normalized spectrum with a width $\Delta\omega$

$$\sigma_{D2}(\omega) = \left[\frac{3}{I_n^2(\omega)}\frac{\Delta\omega^2}{\mathrm{SNR}\,pM(\delta\omega)^6}\right]^{1/2}. \tag{19}$$

As a key result, we find that for a fixed number of data points p and number of averages M, the standard deviation of GDD (σ_{D2}) is proportional to the third power of the inverse spectral resolution. As a consequence, the noise level rises rapidly with improved resolution. To maintain a certain accuracy of GDD determination, one has to strongly increase the number of averages, if the parameters of light source and detection cannot be improved. This shows that a practical limit of achievable spectral resolution in spectrally integrated time-domain white-light interferometry is set by the detection noise and can hardly be pushed by improving the electronics or increasing the measurement time.

5. COMPARISON WITH EXPERIMENT

Using the setup and the algorithm described above, we measured the wavelength-dependent GDD of a multilayer DUT (see Fig. 3). We obtained the GDD values (D_2) and its standard deviation σ_{D2} from M individual scans. The best estimate for D_2 is the average of M individual numbers, whereas the standard deviation σ_{D2} is calculated as the square root of the sum of the squared deviations from the average, divided by the square root of $M(M-1)$. Figure 4 shows experimental results for a constant number of averaged traces but two different wavelength resolutions of 9.1 and 4.0 nm. The large difference in the standard deviations for the GDD is consistent with our predictions [see Eq. (18)].

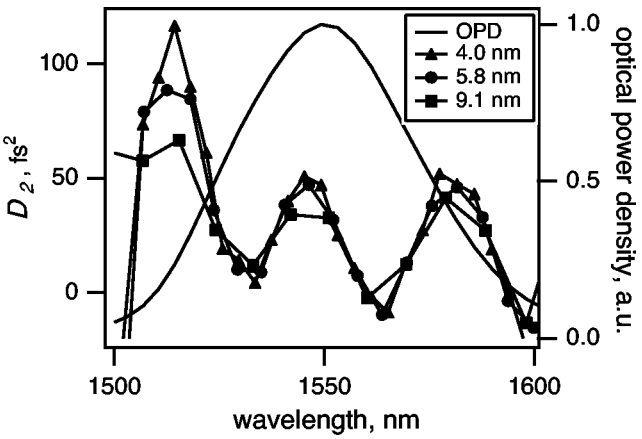

Fig. 3. Optical power density OPD (right axis) and GDD (left axis) of DUT, measured with three different resolutions (9.1, 5.8, and 4.0 nm) and corresponding number of averages (150, 2 313, and 22 048), scaled with the sixth power of the spectral resolution for equal standard deviations of all measurements.

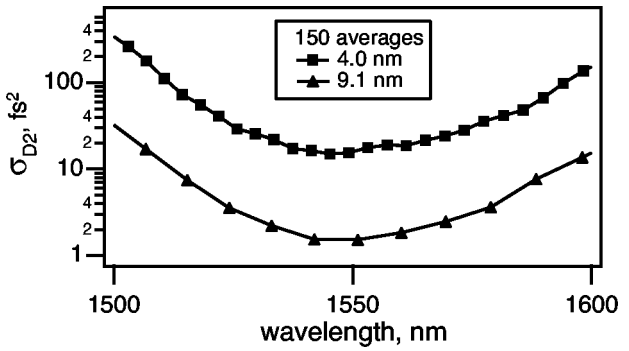

Fig. 4. Standard deviation of measured GDD (σ_{D2}) versus wavelength for a fixed number of averaged traces and two different wavelength resolutions.

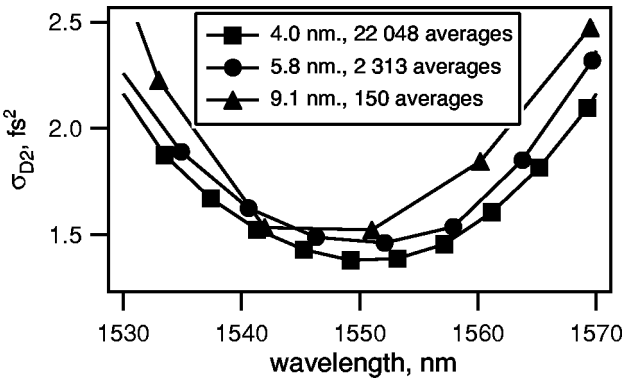

Fig. 5. Experimentally obtained standard deviation of GDD (σ_{D2}) measured with 4.0, 5.8, and 9.1 nm resolution and corresponding number of averages (22 048, 2 313, and 150).

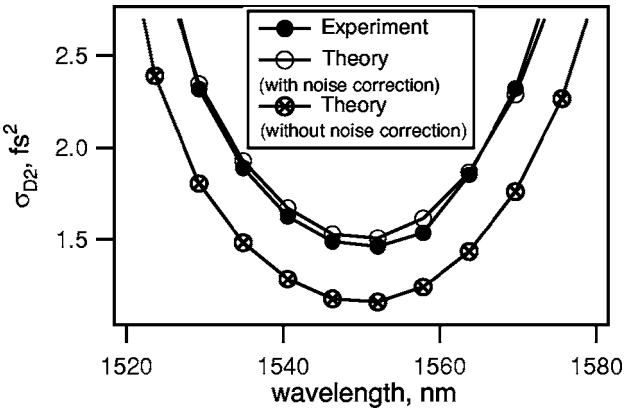

Fig. 6. Standard deviation of GDD (σ_{D2}). Filled circles, experimentally measured with 5.8 nm resolution and 2 313 averages; crossed circles, theoretically calculated value without noise correction; open circles, theoretically calculated value with correction for residual noise correlations.

Figure 3 shows the normalized spectrum of the white light and experimentally obtained values of D_2 versus wavelength, measured for three different resolutions (4.0, 5.8, and 9.1 nm). In this case we have chosen different numbers of averages (22 048, 2 313, and 150), scaled with the sixth power of the inverse spectral resolution, so that the theory predicts equal standard deviations for all measurements.

Figure 5 shows an experimentally obtained standard deviation of GDD (σ_{D2}) versus wavelength for the same three different resolutions and the number of averages as in Fig. 3. Theoretically expected standard deviations, as calculated from Eq. (18), and an experimentally measured value for 5.8 nm resolution and 2 313 averages are shown in Fig. 6. First, the data confirmed that the standard deviation of GDD (σ_{D2}) indeed scales with the third power of the inverse spectral resolution [compare with Eq. (18)], as the obtained standard deviations for the different resolutions are very similar, when the number of averages M is adopted according to Eq. (18). Second, even without precise knowledge of the spectral shape (noise with flat spectral distribution was assumed) the absolute values are in reasonable agreement with the theoretical expectation (see the curve "Theory without noise correction" on Fig. 6).

In order to estimate *SNR* in the time domain [see Eq. (15)], we extracted the amplitude $S_{\max}$ of the cross-correlation envelope (Fig. 2) from the recorded white-light interferograms. The noise level in the time domain can be estimated from the standard deviation σ_s of data points in the wings of the interferogram (large Δz) where the interference signal is much lower than the noise floor (see Fig. 2). Indeed, we found the same noise level on data traces recorded with the white-light source switched off.

So far we have assumed uncorrelated noise in different sample points of the interferograms, which led to white (frequency-independent) noise in the spectral phase. Indeed, the Fourier transform of data traces with the white-light source switched off (or with the arbitrary long offset in the arm length) displays a rather flat spectrum, however, the noise power increases slightly toward lower frequencies, apparently owing to low-frequency electronic noise. The resulting noise in the region of the optical spectra turned out to be about 1.3 times higher than the noise averaged over the whole Fourier-transformed traces. Therefore, using Eq. (18), we underestimated the relevant noise spectral density, which eventually lowered the calculated GDD variances. Using the actual spectral noise density at the interference frequencies, i.e., 1.3 times the average noise power density, we evaluated the actual SNR and found excellent agreement between experimental measurements and the theory, as shown on the Fig. 6 curve "Theory with noise correction."

6. DISCUSSION AND CONCLUSIONS

We have theoretically calculated and experimentally confirmed the effect of noise on dispersion measurements with scanning FT white-light interferometers. The key result is that the precision of GDD determination σ_{D2} scales with the third power of the inverse spectral resolution for a given measurement time and a number of interpolation points, and the measurement time for a given accuracy σ_{D2} scales with the sixth power of the inverse spectral resolution. As a consequence, a fine spectral resolution is very hard to achieve together with a high GDD precision. For example, when a dispersion measurement with 10 nm resolution takes 1 min and the same noise level is to be achieved in a measurement with 1 nm resolution by increasing the number of averaged data traces (with otherwise unchanged conditions), this 1 nm measurement will take two years.

According to Eq. (17), an increase in the number of sampling (interpolation) points p reduces the noise of measured GDD spectra. However, the available sampling memory and computation time set an upper limit for the number of interpolation points.

One may also use multiple passes on the DUT to improve the accuracy, but obviously this method has a limited scope.

Another way to achieve the required improvement of the SNR is to use a white-light source with higher spectral brightness [i.e., $\sigma_{D2}(\omega) \propto I_n(\omega)^{-1}$, according to Eqs. (18) and (19)]. As long as the detection noise is limited by, e.g., the photodetection electronics, but not the digital sampling electronics, the absolute noise level can be considered to be independent of the power level of the source. In that case, doubling the spectral brightness will reduce the standard deviation of the GDD (σ_{D2}) by a factor of 2. In this regime, the bandwidth of the white-light source is not important for the achieved accuracy; doubling the spectral bandwidth $\Delta\omega$ (for a constant spectral brightness) will double the peak value (signal) of the interferograms [see Eq. (15)], but the resulting improvement of the SNR is exactly canceled by the term with $(\Delta\omega)^2$ in the numerator [see Eqs. (18) and (19)]. In other words, the noise in the measured spectral phase for one optical frequency is not affected by power at other frequencies. Measurements based on tungsten bulbs as white-light sources usually operate in this regime.

A different regime is reached once the peak signal of the interferograms gets so high that the noise is limited by the resolution of the analog-to-digital (A/D) converter. In that case, the noise level rises together with the increased signal level, if either the spectral brightness or the bandwidth of the light source is increased. This means that a further increase of spectral brightness does not help, whereas an increase of bandwidth is even detrimental, as it increases the peak signal and thus forces one to measure in a regime with higher noise level. This regime can be reached when a bright white-light source such as, e.g., an SOA, a superluminescent light-emitting diode (SLED), or a broadband laser is used. To overcome the resolution limit imposed by the A/D converters, one can perform highly accurate dispersion evaluation by combining measurements with reduced bandwidth and different optical center frequencies (using a tunable light source or some filters). For example, by reducing the optical bandwidth per measurement by a factor of 10, one could reach a certain noise level with 100 times fewer averaged traces per measurement, i.e., with one tenth of the total measurement time. Similarly, spectrally resolved detection may in this case provide a better noise performance than the spectrally integrated method.

The measurement precision can also depend on the magnitude of the measured GDD, depending on what limits the noise. Obviously, the maximum amplitude of the cross-correlation envelope (S_{max}) gets smaller for larger GDD values. Smaller S_{max} allows for stronger signal amplification. If one is limited by the digitizing noise, the recorded noise level is not affected by the amplification. Consequently, the GDD uncertainty may decrease with an increasing amount of GDD to be measured. However, if digitizing noise is not a limiting factor, the measurement precision does not depend on the amount of GDD.

Finally, we have so far disregarded noise from the white-light source itself. This should usually be a valid approximation, particularly for low-brightness sources such as bulbs and even for high-brightness sources such as SLEDs, but not necessarily for broadband lasers, which can have significant intensity noise. In this situation, a more detailed investigation of the relevant noise contributions is necessary.

Note that spectral interferometry also exhibits an increase of required measurement time with tightened demands on wavelength resolution, although in detail the limitations are different, and there are additional problems related to these techniques,[27] such as, e.g., linearity of wavelength calibration, evaluation of the delay time in connection with the SNR, determination of the spectrometer response function, pixelation errors of the detector, filtering, spatial problems, calibration error related to delay-dependent error in the retrieved phase, etc. Therefore spectrally integrated interferometry, as discussed in this paper, may often be preferred over the more sophisticated spectrally resolved techniques.

ACKNOWLEDGMENT

This work was supported by the Swiss National Science Foundation (NCCR).

A. Gosteva is the corresponding author and can be reached by e-mail at gosteva@phys.ethz.ch, by phone at +41 44 633 29 53, or by fax at +41 44 633 10 59.

REFERENCES

1. I. Walmsley, L. Waxer, and C. Dorrer, "The role of dispersion in ultrafast optics," Rev. Sci. Instrum. **72**, 1–29 (2001).
2. D. H. Sutter, L. Gallmann, N. Matuschek, F. Morier-Genoud, V. Scheuer, G. Angelow, T. Tschudi, G. Steinmeyer, and U. Keller, "Sub-6-fs pulses from a SESAM-assisted Kerr-lens modelocked Ti:sapphire laser: at the frontiers of ultrashort pulse generation," Appl. Phys. B **70**, S5–S12 (2000).
3. G. Steinmeyer, D. H. Sutter, L. Gallmann, N. Matuschek, and U. Keller, "Frontiers in ultrashort pulse generation: pushing the limits in linear and nonlinear optics," Science **286**, 1507–1512 (1999).
4. N. Matuschek, L. Gallmann, D. H. Sutter, G. Steinmeyer, and U. Keller, "Back-side-coated chirped mirrors with ultra-smooth broadband dispersion characteristics," Appl. Phys. B **71**, 509–522 (2000).
5. G. Sansone, G. Steinmeyer, C. Vozzi, S. Stagira, M. Nisoli, S. De Silvestri, K. Starke, D. Ristau, B. Schenkel, J. Biegert, A. Gosteva, and U. Keller, "Mirror dispersion control of a hollow fiber supercontinuum," Appl. Phys. B **78**, 551–555 (2004).
6. B. Schenkel, R. Paschotta, and U. Keller, "Pulse compression with supercontinuum generation in microstructure fibers," J. Opt. Soc. Am. B **22**, 687–693 (2005).
7. M. Zavelani-Rossi, G. Cerullo, S. De Silvestri, L. Gallmann, N. Matuschek, G. Steinmeyer, U. Keller, G. Angelow, V. Scheuer, and T. Tschudi, "Pulse compression over a 170-THz bandwidth in the visible by use of only chirped mirrors," Opt. Lett. **26**, 1155–1157 (2001).
8. B. Schenkel, J. Biegert, U. Keller, C. Vozzi, M. Nisoli, G.

Sansone, S. Stagira, S. De Silvestri, and O. Svelto, "Generation of 3.8-fs pulses from adaptive compression of a cascaded hollow fiber supercontinuum," Opt. Lett. **28**, 1987–1989 (2003).
9. A. Baltuska, T. Fuji, and T. Kobayashi, "Visible pulse compression to 4 fs by optical parametric amplification and programmable dispersion control," Opt. Lett. **27**, 306–308 (2002).
10. M. Nisoli, S. De Silvestri, O. Svelto, R. Szipcs, K. Ferencz, Ch. Spielmann, S. Sartania, and F. Krausz, "Compression of high-energy laser pulses below 5 fs," Opt. Lett. **22**, 522–524 (1997).
11. L. Gallmann, G. Steinmeyer, G. Imeshev, J.-P. Meyn, M. M. Fejer, and U. Keller, "Sub-6-fs blue pulses generated by quasi-phase-matching second-harmonic generation pulse compression," Appl. Phys. B **74**, S237–S243 (2002).
12. K. Yamane, Z. G. Zhang, K. Oka, R. Morita, M. Yamashita, and A. Suguro, "Optical pulse compression to 3.4 fs in the monocycle region by feedback phase compensation," Opt. Lett. **28**, 2258–2260 (2003).
13. C. P. Hauri, W. Kornelis, F. W. Helbing, A. Heinrich, A. Couairon, A. Mysyrowicz, J. Biegert, and U. Keller, "Generation of intense, carrier-envelope phase-locked few-cycle laser pulses through filamentation," Appl. Phys. B **79**, 673–677 (2004).
14. L. Gallmann, G. Steinmeyer, D. H. Sutter, N. Matuschek, and U. Keller, "Collinear type II second-harmonic-generation frequency-resolved optical gating for the characterization of sub-10-fs optical pulses," Opt. Lett. **25**, 269–271 (2000).
15. L. Gallmann, D. H. Sutter, N. Matuschek, G. Steinmeyer, U. Keller, C. Iaconis, and I. A. Walmsley, "Characterization of sub-6-fs optical pulses with spectral phase interferometry for direct electric-field reconstruction," Opt. Lett. **24**, 1314–1316 (1999).
16. L. Gallmann, D. H. Sutter, N. Matuschek, G. Steinmeyer, and U. Keller "Techniques for the characterization of sub-10-fs optical pulses: a comparison," Appl. Phys. B **70**, S67–S75 (2000).
17. M. Kuznetsov, F. Hakimi, R. Sprague, and A. Mooradian, "Design and characteristics of high-power (>0.5-W CW) diode-pumped vertical-external-cavity surface-emitting semiconductor lasers with circular TEM00 beams," IEEE J. Sel. Top. Quantum Electron. **5**, 561–573 (1999).
18. R. Haring, R. Paschotta, A. Aschwanden, E. Gini, F. Morier-Genoud, and U. Keller, "High-power passively mode-locked semiconductor lasers," IEEE J. Quantum Electron. **38**, 1268–1275 (2002)
19. U. Keller, K. J. Weingarten, F. X. Kärtner, D. Kopf, B. Braun, I. D. Jung, R. Fluck, C. Hönninger, N. Matuschek, and J. Aus der Au, "Semiconductor saturable absorber mirrors (SESAMs) for femtosecond to nanosecond pulse generation in solid-state lasers," IEEE J. Sel. Top. Quantum Electron. **2**, 435–453 (1996).
20. K. Naganuma, K. Mogi, and H. Yamada, "Group-delay measurement using the Fourier transform of an interferometric cross correlation generated by white light," Opt. Lett. **15**, 393–395 (1990).
21. S. Diddams and J.-C. Diels, "Dispersion measurements with white-light interferometry," J. Opt. Soc. Am. B **13**, 1120–1129 (1996).
22. C. Dorrer, N. Belabas, J-P. Likforman, and M. Joffre, "Experimental implementation of Fourier-transform spectral interferometry and its application to the study of spectrometers," Appl. Phys. B **70**, S99–S107 (2000).
23. C. Dorrer and F. Salin, "Characterization of spectral phase modulation by classical and polarization spectral interferometry," J. Opt. Soc. Am. B **15**, 2331–2337 (1998).
24. M. Beck and I. A. Walmsley, "Measurement of group delay with high temporal and spectral resolution," Opt. Lett. **15**, 492–494 (1990).
25. M. Beck, I. A. Walmsley, and J. D. Kafka, "Group delay measurements of optical components near 800 nm," IEEE J. Quantum Electron. **27**, 2074–2081 (1991).
26. A. P. Kovacs, K. Osvay, Z. Bor, and R. Szipocs, "Group-delay measurement on laser mirrors by spectrally resolved white-light interferometry," Opt. Lett. **20**, 788–790 (1995).
27. C. Dorrer, "Influence of the calibration of the detector on spectral interferometry," J. Opt. Soc. Am. B **16**, 1160–1168 (1999).
28. M. Takeda, H. Ina, and S. Kobayashi, "Fourier-transform method of fringe-pattern analysis for computer-based topography and interferometry," J. Opt. Soc. Am. **72**, 156–160 (1982).